Semi-Dirac point in the Hofstadter spectrum

P. Delplace and G. Montambaux
Laboratoire de Physique des Solides, CNRS UMR 8502, Université Paris-Sud, 91405-Orsay, France
(Received 1 February 2010; published 28 July 2010)

The spectrum of tight-binding electrons on a square lattice with half a magnetic-flux quantum per unit cell exhibits two Dirac points at the band center. We show that, in the presence of an additional uniaxial staggered potential, this pair of Dirac points may merge into a single one with a topological transition toward a gapped phase. At the transition, the spectrum is linear in one direction and quadratic in the other one (a spectrum recently named "hybrid" or "semi-Dirac"). This transition is studied in the framework of a general Hamiltonian describing the merging of Dirac points. The possibility of creating gauge fields for cold atoms in optical lattices may offer an opportunity to observe this merging of Dirac points and the hybrid dispersion relation.

DOI: 10.1103/PhysRevB.82.035438 PACS number(s): 37.10.Jk, 73.43.−f

I. INTRODUCTION

Condensed matter offers the possibility of manipulating the energy spectrum of electrons and modifying their free dispersion relation. Band theory leads to complex dispersion relations, commonly with *quadratic* expansions in the vicinity of peculiar symmetry points. These quadratic expansions are characterized by a tensor of effective masses, possibly with positive and negative masses (near a saddle point). Graphene offers the exciting situation where the dispersion relation at low energy is *linear*, similar to the spectrum of relativistic particles described by the Dirac equation.[1,2] More precisely, the spectrum has the form of two cones (the so-called "Dirac cones" or "Dirac points") in the vicinity of the $\boldsymbol{K}$ and $\boldsymbol{K}'$ points of the reciprocal space. It has been recently proposed and studied the existence of a *hybrid* spectrum, quadratic in one direction and linear in the other one with interesting consequences for the energy spectrum of Landau levels in the presence of a magnetic field.[3] Such a spectrum may appear in a hypothetical graphenelike structure where one t' of the hopping integrals t between nearest neighbors is increased.[4–10] By doing so, the two Dirac points move and, for a critical value of this hopping integral ($t'=2t$), they merge into a single one with the peculiar hybrid spectrum.

Other possible systems exhibiting a hybrid spectrum have been proposed including the organic conductor α-(BEDT-TTF)$_2$I$_3$,[11–13] VO_2/TiO_2 nanostructures.[14] In the context of VO_2/TiO_2 nanostructures, the hybrid point has been baptized a "semi-Dirac" point,[14] a name that we will use in this paper. Quite recently, one of us has proposed a general framework to study the motion and the merging of Dirac points in two-dimensional (2D) crystals with time-reversal and inversion symmetries, within the framework of the following Hamiltonian:[7,9]

$$\mathcal{H}(\mathbf{q}) = \begin{pmatrix} 0 & \Delta + \dfrac{q_\parallel^2}{2m^*} - ic_\perp q_\perp \\ \Delta + \dfrac{q_\parallel^2}{2m^*} + ic_\perp q_\perp & 0 \end{pmatrix}, \quad (1)$$

where, by varying the product $m^*\Delta$ from negative to positive values, a topological transition separates a phase with two Dirac points from a gapped phase with a semi-Dirac spectrum at the transition, i.e., when $\Delta=0$. This Hamiltonian is universal in the sense that the parameters do not refer to a specific crystal and can be related to the microscopic parameters of any 2D system. It has been shown that in a magnetic field B, the Landau-level spectrum evolves continuously from a $\sqrt{nB}$ dependence to a linear $(n+1/2)B$ behavior with a $[(n+1/2)B]^{2/3}$ dependence at the transition.[3,7,9]

At the moment, there is no straightforward experimental evidence for such merging of Dirac points in electronic systems. A very interesting alternative is the possibility of fabricating a "crystal" of cold atoms in an artificial optical lattice. Two types of systems have been proposed:

The first one is to trap cold atoms in an optical *honeycomb lattice* and thus simulate graphene physics.[15–17] Two recent extensive studies have shown the possibility of tuning the position of the Dirac points by changing the intensity of the laser fields.[15,17]

The second proposal concerns the square lattice.[19–21] In this case, it is known for electronic systems that a Dirac spectrum is obtained in the presence of a magnetic field corresponding to a half-flux quantum per elementary plaquette (the so-called π phase because the total phase accumulated by the electron around the plaquette is π). A major complication stems from the fact that the atoms are neutral and are not coupled to a magnetic field. However, a fictitious magnetic field can be induced by a rotation of the sample (then the role of the magnetic field is played by the Coriolis force[18]) or by effective gauge potentials.[19] Quite recently, a detailed experimental scheme has been proposed, to simulate massless Dirac Fermions on a square lattice by creating a fictitious half-flux quantum per plaquette.[19–21] Note that it has also been proposed that by sweeping the amplitude of the gauge fields, it should be even possible to reveal the full Hofstadter spectrum.[19,22] The main goal of our paper is to propose a mechanism of merging of the Dirac points for cold atoms on a square lattice. The mechanism is quite different from the case of the honeycomb lattice. Whereas in the latter, the merging transition is driven by a variation in some of the nearest-neighbor hopping integrals, which may be difficult to achieve experimentally, here we propose a simple staggered on-site potential as the driving parameter.

The so-called Hofstadter spectrum represents the energy levels of two-dimensional electrons on a square lattice in a magnetic field within the nearest-neighbor tight-binding model.[23] The spectrum depends on the value of the magnetic flux ϕ through an elementary plaquette of the lattice. For rational values of the reduced magnetic flux, $\varphi=\phi/\phi_0=p/q$, $\phi_0=h/e$ being the flux quantum, the electronic spectrum consists of q subbands, leading to the famous fractal structure of the spectrum.

It is well-known that for a half-flux quantum, $\phi=\phi_0/2=h/2e$, the spectrum exhibits two Dirac cones at the band center, quite similarly to the spectrum of graphene. One may wonder if these two Dirac points can be manipulated (moved and merged) by some additional parameter, somehow similarly to the modification of the transfer integrals in the honeycomb lattice. In this paper, we show that an appropriate additional parameter is a staggered potential applied along one direction. The addition of this uniaxial staggered potential modifies the position of the Dirac points which may eventually merge into a "hybrid/semi-Dirac" point for a critical value of the potential. The structure of the paper is the following. In Sec. II, we review the basic equations for electrons on a square lattice in a magnetic field and a uniaxial staggered potential. We discuss the general structure of the resulting Hofstadter spectrum. After a brief analysis of the low-field spectrum (Sec. III), we present our main results in Sec. IV on the evolution of the spectrum for a flux in the vicinity of $\phi_0/2$. After a short analysis of the spectrum near the extrema of the band, we study the spectrum near the center of the band ($\epsilon=0$). For $\phi_0/2$, it consists of two Dirac cones which merge for a critical value of the staggered potential. Using the mapping to an effective Hamiltonian near $\epsilon=0$, we describe *quantitatively* the evolution of the Landau levels in the vicinity of $\phi_0/2$. We conclude in Sec. V.

II. BUTTERFLY SPECTRUM WITH A UNIAXIAL STAGGERED POTENTIAL

We consider the problem of tight-binding electrons on a square two-dimensional lattice. The sites are written as $x=ma$ and $y=na$, a being the lattice spacing. In addition, we apply a uniaxial staggered potential of the form $(-1)^m\Delta_s$ along the x direction, as illustrated in Fig. 1. The unit cell is made of two atoms having different site energies $\pm\Delta_s$. In the presence of a perpendicular magnetic field B, using the Landau gauge where $A_y=Bx$, the Schrödinger equation reads

$$\epsilon\phi_{m,n} = -t\phi_{m,n+1}e^{-2i\pi m\varphi} - t\phi_{m,n-1}e^{2i\pi m\varphi} - t\phi_{m+1,n} - t\phi_{m-1,n} + (-1)^m\Delta_s\phi_{m,n}, \quad (2)$$

where $\phi_{m,n}$ is the amplitude of the wave function on site (m,n), t is the hopping integral between nearest neighbors, and $\varphi=eBa^2/h$ is the dimensionless flux through an elementary plaquette of the lattice. Consider the case of a commensurate flux $\varphi=p/q$ where q is even. There are q inequivalent sites in the unit cell, which is now q times larger along the x direction. We introduce a cell index l so that $m=ql+j$, where

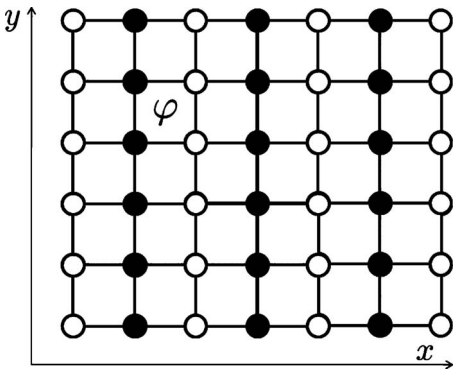

FIG. 1. Square lattice in a uniform magnetic field and a uniaxial staggered potential along the x direction. The black and white disks represent the on-site potentials $\pm\Delta_s$. φ is the dimensionless flux per plaquette.

j is the position of the site in the unit cell: $j=1,\ldots,q$. Since there are q sites per unit cell, the Brillouin zone in the x direction is q times smaller and Bloch's theorem implies that

$$\phi_{m,n} = \phi_{l,n}^{(j)} = \psi_{\boldsymbol{k}}^{(j)}e^{i(k_x lq+k_y n)a} \quad (3)$$

with $\boldsymbol{k}=(k_x,k_y)$ and we have

$$\psi_{\boldsymbol{k}}^{(q+1)} = \psi_{\boldsymbol{k}}^{(1)}. \quad (4)$$

The Schrödinger equation now reads

$$\epsilon\psi_{\boldsymbol{k}}^{(j)} = -t\psi_{\boldsymbol{k}}^{(j+1)} - t\psi_{\boldsymbol{k}}^{(j-1)} - 2t\psi_{\boldsymbol{k}}^{(j)}\cos(k_y a - 2\pi j\varphi) + (-1)^j\Delta_s\psi_{\boldsymbol{k}}^{(j)}, \quad (5)$$

$$\epsilon\psi_{\boldsymbol{k}}^{(1)} = -t\psi_{\boldsymbol{k}}^{(2)} - t\psi_{\boldsymbol{k}}^{(q)}e^{-iqk_x a} - 2t\psi_{\boldsymbol{k}}^{(1)}\cos(k_y a - 2\pi\varphi) - \Delta_s\psi_{\boldsymbol{k}}^{(1)}, \quad (6)$$

$$\epsilon\psi_{\boldsymbol{k}}^{(q)} = -t\psi_{\boldsymbol{k}}^{(q-1)} - t\psi_{\boldsymbol{k}}^{(1)}e^{iqk_x a} - 2t\psi_{\boldsymbol{k}}^{(q)}\cos(k_y a - 2\pi q\varphi) + (-1)^q\Delta_s\psi_{\boldsymbol{k}}^{(q)}. \quad (7)$$

This is a $q\times q$ system with q eigenvalues. If q is odd, sites with even and odd m are inequivalent, and the unit cell has a size $2qa$ in the x direction. Equations (6)–(8) are unchanged (except $q\to 2q$ since $j=1,\ldots,2q$) and $\psi_{\boldsymbol{k}}^{(2q+1)}=\psi_{\boldsymbol{k}}^{(1)}$.

The Fig. 2 present the evolution of the spectrum (energy in units of t versus magnetic flux) when the staggered potential Δ_s is increased. Figure 2(a) is the familiar Hofstadter spectrum obtained for $\Delta_s=0$. Figure 2(b) shows the spectrum for $\Delta_s=t$. The most striking difference between Figs 2(a) and 2(b) is that many gaps have been filled. This is even more spectacular in Fig. 2(c), corresponding to the critical value $\Delta_s=2t$ of the staggered potential for which the Dirac points in the $\varphi=1/2$ dispersion relation merge, as we will see later.[24] This suppression of many gaps is qualitatively understood by the fact that, when Δ_s increases, there are more and more open classical orbits which are not quantized, as we discuss in Sec. III A.

The main goal of our paper is the study of the spectrum near half-flux quantum $\varphi=1/2$, near the center of the band.

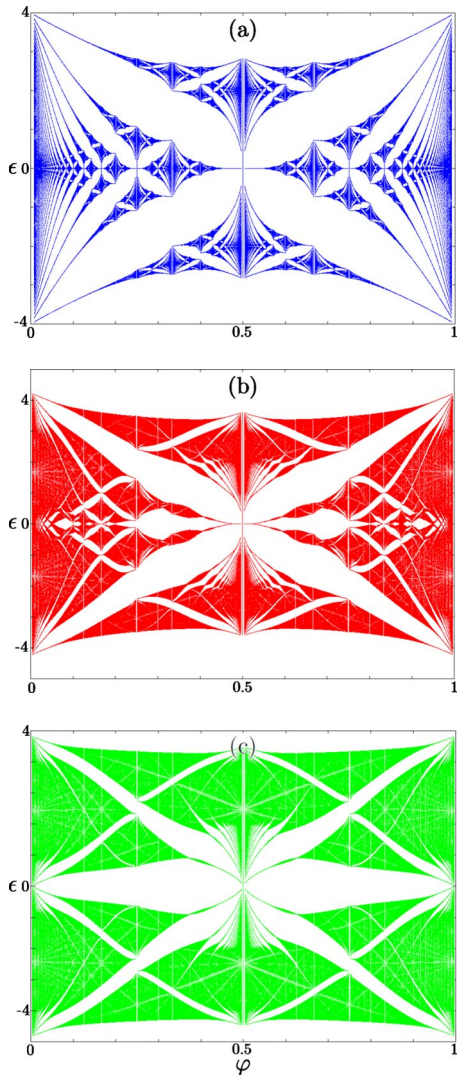

FIG. 2. (Color online) Evolution of the Hofstadter spectrum for the square lattice, in the presence of a uniaxial staggered on-site potential characterized by the parameter $r=\Delta_s/(2t)$. (a) $r=0$, this is the usual Hofstadter spectrum. In the center of the band ($\epsilon=0$) near $\varphi=1/2$, the energy levels vary as $\sqrt{nf}$, where $f=|\varphi-1/2|$. (b) $r=1/2$, the degeneracy of the levels near $\epsilon=0$, $\varphi=1/2$ has been lifted. (c) Spectrum at the critical point $r=1$. The levels near $\epsilon=0$, $\varphi=1/2$ vary as $[(n+1/2)f]^{2/3}$.

For $\Delta_s=0$, this spectrum is quite similar to the low-field spectrum of graphene: due to the presence of two Dirac points, the spectrum near $\varphi=1/2$ consists of a series of Landau levels varying as $\sqrt{nf}$, where $f=|\varphi-1/2|$ is the deviation from $\varphi=1/2$ [Fig. 2(a)]. These Landau levels are doubly degenerate due to the twofold degeneracy of the Dirac spectrum. When Δ_s increases, the degeneracy is progressively lifted [Fig. 2(b)] and at the critical point $\Delta_s=2$ [Fig. 2(c)], the levels vary as $[(n+1/2)f]^{2/3}$, as we will show in Sec. IV C. Then, for $\Delta_s>2$, a gap opens and the Landau levels progressively evolve toward a linear variation as $(n+1/2)f$. We now discuss the different parts of the spectrum and their evolution when the staggered potential Δ_s is increased.

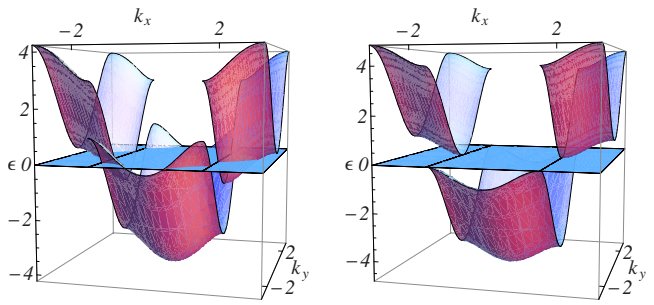

FIG. 3. (Color online) Zero-field spectrum $\epsilon(\boldsymbol{k})$ for tight-binding electrons on the square lattice with a staggered potential. The two bands overlap when $r<1$. Left panel: $r=0.5$. Right panel: when $r=1$, the two bands no longer overlap. We have represented the plane $\epsilon=0$.

III. LOW-FIELD SPECTRUM

A. Zero-field spectrum

In zero field due to the staggered potential, the Hamiltonian has a 2×2 structure

$$\mathcal{H}(\boldsymbol{k}) = -2\begin{pmatrix} \cos k_y - r & \cos k_x \\ \cos k_x & \cos k_y + r \end{pmatrix}, \tag{8}$$

where we introduce the dimensionless parameter $r=\Delta_s/(2t)=\Delta_s/2$ and where we choose from now $t=a=\hbar=e=1$. Therefore the zero-field spectrum is given by

$$\epsilon(\boldsymbol{k}) = -2\cos k_y \pm 2\sqrt{\cos^2 k_x + r^2}. \tag{9}$$

As shown in Fig. 3, the spectrum consists of two bands which overlap in energy. The lower band extends from $\epsilon_l^{min}=-2-2\sqrt{1+r^2}$ to $\epsilon_l^{max}=2-2r$ with two saddle points (which yields logarithmic singularities in the density of states) at energies $\epsilon_l^{s1}=-2-2r$ and $\epsilon_l^{s2}=+2-2\sqrt{1+r^2}$. Symmetrically, the upper band extends from $\epsilon_u^{min}=-2+2r$ to $\epsilon_u^{max}=2+2\sqrt{1+r^2}$ with two saddle points (with logarithmic singularities) at energies $\epsilon_u^{s1}=-2+2\sqrt{1+r^2}$ and $\epsilon_u^{s2}=2+2r$. The position of these points is shown on Fig. 4 on a plot of the density of states.

In each band, the saddle points separate regions with open orbits (for energies between the two saddle points) and closed orbits. When $\Delta_s=0$, all orbits are closed and the total bandwidth for incommensurate fluxes is zero. This can be qualitatively understood on semiclassical grounds: all closed orbits are quantized and magnetic breakdown induces tunneling between orbits which are all quantized.[25] When Δ_s increases, there are open orbits which are not quantized and the total bandwidth for incommensurate fluxes increases like the number of open orbits.[25] This qualitatively explains why the spectrum is more and more dense when Δ_s increases.

B. Low field spectrum, at the edges of the band

At low-magnetic field ($\varphi\ll1$), the energy levels near the extrema of the band, are grouped into linear Landau levels

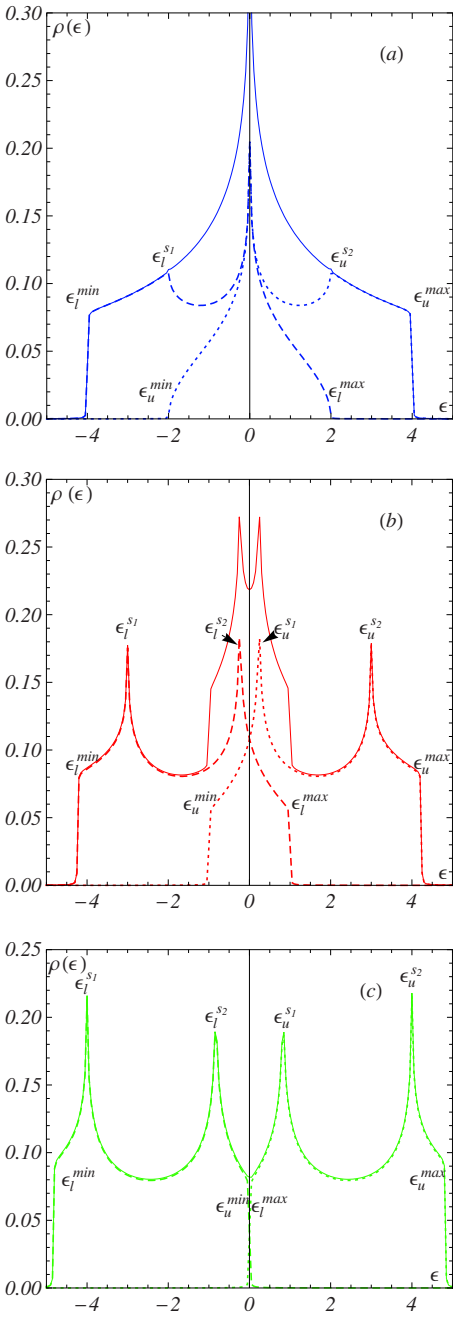

FIG. 4. (Color online) Zero-field density of states for tight-binding electrons on a square lattice with a staggered potential, corresponding to the dispersion relation Eq. (9) for (a) $r=0$, (b) $r=0.5$, and (c) $r=1$. We have plotted the density of states in the lower band (dashed line), the density of states in the upper band (dotted line), and the total density of states (full line).

(Fig. 2). Their spectrum is obtained from a low-energy expansion of the dispersion relation Eq. (9) near $\boldsymbol{k}=0$

$$\epsilon(\boldsymbol{k}) = \mp 2(1+\sqrt{1+r^2}) \pm \left(\frac{k_x^2}{\sqrt{1+r^2}} + k_y^2\right) + \cdots \quad (10)$$

leading to a cyclotron mass $m_0=(1+r^2)^{1/4}/2$ and therefore to a set of Landau levels given by ($B=2\pi\varphi$ in our notations)

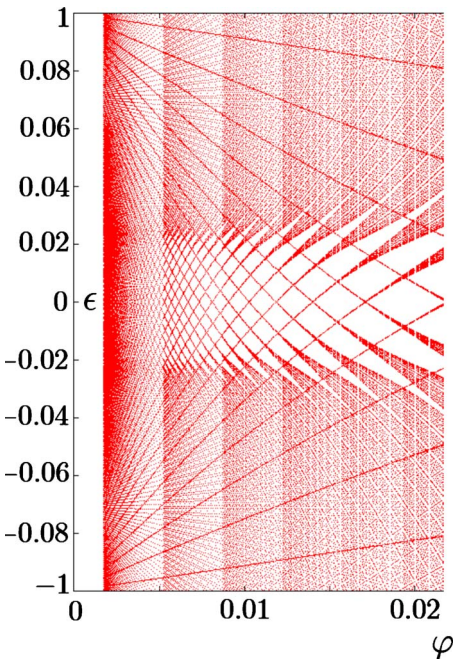

FIG. 5. (Color online) Low field part of the Hofstadter spectrum $\epsilon(\varphi)$, in the presence of a uniaxial potential with $r=0.5$, in the energy range $[-1,1]$. The intermixing of the Landau levels is described in the text and given analytically by Eq. (13).

$$\epsilon_n(\varphi) = \mp (2+2\sqrt{1+r^2}) \pm \frac{4\pi}{(1+r)^{1/4}}\left(n+\frac{1}{2}\right)\varphi + \cdots, \quad (11)$$

which describes properly the evolution of the Landau levels at the extrema of the spectrum (Fig. 2).

C. Low field spectrum, center of the band

Figure 2(b) shows that, in the middle of the band and for a finite Δ_s, two set of Landau levels intermix. This is emphasized in the enlargement displayed in Fig. 5. This structure is easily understood by looking at the zero-field spectrum, displayed on Fig. 3. When $0<r<1$, the spectrum is formed of two overlapping bands. The maximum of the lower band is located at energy $\epsilon=2(1-r)$ and the minimum of the upper band has energy $\epsilon=-2(1-r)$. An expansion around these energies gives

$$\epsilon(\boldsymbol{q}_\pm) = \mp 2(1-r) \pm \left(k_y^2 + \frac{k_x^2}{r}\right) + \cdots, \quad (12)$$

where $\boldsymbol{q}_\pm$ are deviations, respectively, to the points $(\pi/2,0)$ and $(\pi/2,\pi)$. Therefore the cyclotron mass scales as $m_0=\sqrt{r}/2$, and the two sets of Landau levels are given by

$$\epsilon_n(\varphi) = \mp 2(1-r) \pm \frac{4\pi}{\sqrt{r}}\left(n+\frac{1}{2}\right)\varphi + \cdots. \quad (13)$$

When $r=1$, the two sets of Landau levels separate [Fig. 2(c)].

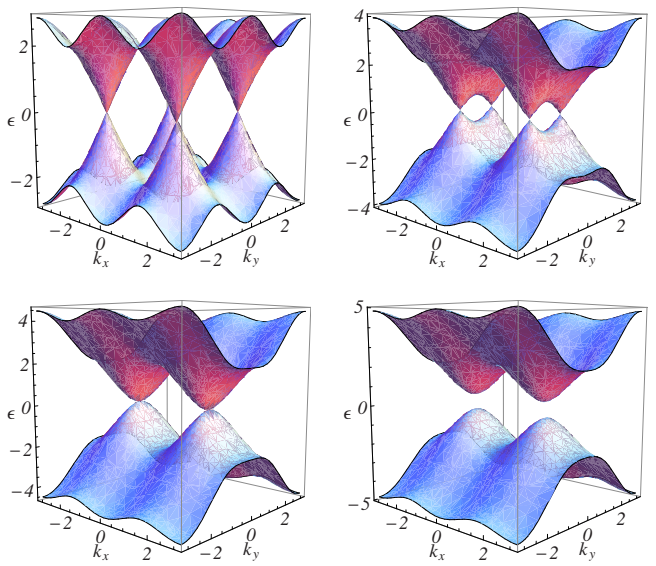

FIG. 6. (Color online) Evolution of the electronic spectrum at $\varphi=1/2$, when a uniaxial staggered potential $(-1)^m\Delta_s$ is added. The four plots correspond, respectively, to $r=\Delta_s/2=0$, 0.7, 1, and 1.2. Note that along the k_x direction, we have represented two Brillouin zones, the first zone being $[-\pi/2,\pi/2]$.

IV. SPECTRUM NEAR $\varphi=1/2$

We now concentrate on the region of the butterfly spectrum near $\varphi=1/2$. Its peculiar structure can be explained from the spectrum precisely *at* $\varphi=1/2$, which plays the role of a zero-flux spectrum perturbed by a small magnetic effective flux $f=|\varphi-1/2|$, corresponding to an effective magnetic field $B_f=2\pi f$ (the real field being $\pi+B_f$ in our units). We first describe the low energy part of the spectrum. Then we study the vicinity of the band center where the spectrum consists in two Dirac cones which progressively merge when the staggered potential increases until the value $r=1$.

A. Spectrum for $\varphi=1/2$

For $\varphi=p/q=1/2$, the Hamiltonian has the form

$$\mathcal{H}(\boldsymbol{k}) = -\begin{pmatrix} 2(\cos k_y - r) & 1+e^{-2ik_x} \\ 1+e^{2ik_x} & 2(r-\cos k_y) \end{pmatrix} \tag{14}$$

with $r=\Delta_s/2$. The energy spectrum given by

$$\epsilon(\boldsymbol{k}) = \pm 2\sqrt{\cos^2 k_x + (\cos k_y - r)^2} \tag{15}$$

is plotted on Fig. 6 for different values of r. It exhibits a pair of Dirac points and their merging occurs when $r=1$.

B. Spectrum near $\varphi=1/2$, low energy

An expansion of the dispersion relation Eq. (15) near its extrema at $\boldsymbol{k}_m=(0,\pi)$ gives $(\boldsymbol{q}=\boldsymbol{k}-\boldsymbol{k}_m)$

$$\epsilon(\boldsymbol{k}_m+\boldsymbol{q}) = \mp 2\sqrt{2+2r+r^2} \pm \frac{q_x^2+(1+r)q_y^2}{\sqrt{2+2r+r^2}} + \cdots . \tag{16}$$

The cyclotron mass m_0 is therefore

$$m_0 = \frac{\sqrt{2+2r+r^2}}{2\sqrt{1+r}} \tag{17}$$

so that in low "flux" f

$$\epsilon_n(f) = \mp 2\sqrt{2+2r+r^2} \pm 4\pi\sqrt{\frac{1+r}{2+2r+r^2}}\left(n+\frac{1}{2}\right)f + \cdots . \tag{18}$$

C. Spectrum near $\varphi=1/2$, center of the band: Dirac points and their merging

This study is the central point of our paper. When $r=0$, the energy vanishes at the two inequivalent points $\boldsymbol{D}_\xi=(\pi/2,\xi\pi/2)$ where $\xi=\pm 1$ is the valley index. In the vicinity of these two points, writing $\boldsymbol{k}=\boldsymbol{D}_\xi+\boldsymbol{q}$, the Hamiltonian can be expanded as

$$\mathcal{H}(\boldsymbol{D}_\xi+\boldsymbol{q}) = 2\begin{pmatrix} \xi q_y & -iq_x \\ iq_x & -\xi q_y \end{pmatrix}. \tag{19}$$

In each valley, the dispersion relation around $\boldsymbol{D}_\xi$ is

$$\epsilon(\boldsymbol{D}_\xi+\boldsymbol{q}) = 2\xi q, \tag{20}$$

as can be seen on Fig. 6(a).

We now apply a finite uniaxial staggered potential $\Delta_s \neq 0$. The Dirac points move and are now located at the positions $\boldsymbol{D}_\xi=(\pi/2,\xi\arccos r)$ [see Fig. 6(b)]. A second-order expansion around these two points leads to

$$\mathcal{H}(\boldsymbol{D}_\xi+\boldsymbol{q}) = 2\begin{pmatrix} \xi\sqrt{1-r^2}q_y + r\dfrac{q_y^2}{2} & -iq_x \\ iq_x & -\xi\sqrt{1-r^2}q_y - r\dfrac{q_y^2}{2} \end{pmatrix} \tag{21}$$

with a dispersion relation at small $\boldsymbol{q}$ of the form

$$\epsilon(\boldsymbol{D}_\xi+\boldsymbol{q}) = \xi\sqrt{c_x^2q_x^2+c_y^2q_y^2} \tag{22}$$

with $c_x=2$ and $c_y=2\sqrt{1-r^2}$.

When r is increased, the two cones become anisotropic because the velocity along the y direction relating the two cones is reduced [Fig. 6(b)]. When $r=1$, the two cones have merged into a single one at the point $\boldsymbol{D}_0=(\pi/2,0)$ [Fig. 6(c)] and the Hamiltonian becomes

$$\mathcal{H}_0(\boldsymbol{q}) = 2\begin{pmatrix} \dfrac{q_y^2}{2} & -iq_x \\ iq_x & -\dfrac{q_y^2}{2} \end{pmatrix} \tag{23}$$

leading to the "hybrid" dispersion relation

$$\epsilon(\boldsymbol{q}) = \pm 2\sqrt{q_x^2+q_y^4/4}. \tag{24}$$

Quite remarkably, this dispersion relation is linear in one direction and quadratic in the other. The study of this semi-Dirac point has been the subject of a series of recent

works[3–10,26] and the present problem constitutes a new realization of this merging.

We now wish to describe the physics of the merging, using the effective Hamiltonian

$$\mathcal{H} = \begin{pmatrix} \Delta + \frac{q_\parallel^2}{2m^*} & -ic_\perp q_\perp \\ ic_\perp q_\perp & -\Delta - \frac{q_\parallel^2}{2m^*} \end{pmatrix} \tag{25}$$

with $q_\parallel = q_y$ and $q_\perp = q_x$. Within the rotation in Hilbert space

$$R = \frac{1}{\sqrt{2}}(\mathbb{I} - i\sigma_y) \quad \text{where} \quad \sigma_y = \begin{pmatrix} 0 & -i \\ i & 0 \end{pmatrix}$$

is a Pauli matrix, it is identical with the universal Hamiltonian (1) that has been recently introduced to describe the merging of Dirac points in a 2D crystal with time-reversal and inversion symmetries. When $m^*\Delta > 0$, there is a gap in the spectrum. Comparison between Eq. (25) and the expansion of Eq. (14) near $\boldsymbol{D}_0$ implies that $\Delta = 2(r-1)$. When $m^*\Delta < 0$, the spectrum has two Dirac points separated by $2\sqrt{-2m^*\Delta}$ and the velocity $c_\parallel$ near these Dirac points is $c_\parallel = \sqrt{-2\Delta/m^*}$.

In order to quantitatively describe the merging of the Dirac points from the Hofstadter spectrum ($r=0$) to the topological transition ($r=1$), we choose to fix the velocities $c_\parallel = c_y = 2\sqrt{1-r^2}$ and $c_\perp = c_x = 2$. Then, the mass m^* has to be fixed as $m^* = -2\Delta/c_\parallel^2 = 1/(1+r)$. The position of the Dirac points is given by $q_D = \pm 2\sqrt{\frac{1-r}{1+r}}$ slightly different from the real position $q_D = \pm \arccos r$ (see Ref. 9, for a discussion on this choice).

Using the universal Hamiltonian (25) whose properties are known in a magnetic field, we now describe the evolution of the spectrum when approaching the merging. When r is small, the spectrum near $\epsilon = 0$ can still be described as two independent cones with modified velocities $c_\perp = 2$ and $c_\parallel = 2\sqrt{1-r^2}$. It is known that in this case,[27] the spectrum is quantized in twofold degenerate (due to the valley degeneracy) Landau levels with the dispersion relation $\epsilon_n = \pm\sqrt{2nc_\parallel c_\perp eB}$. In our notations, this gives

$$\epsilon_n(f) = \pm 4(1-r^2)^{1/4}\sqrt{\pi n f} \tag{26}$$

as confirmed on Figs. 7(a) and 7(b). When r increases, the domain of validity of this expression is reduced. As seen in Figs. 2(b) and 7(b), the twofold degeneracy of the Landau levels is removed when f is increased (in particular the $n=0$ level) until for $r=1$, the degeneracy is completely removed with a new field dependence of the levels.

When $r=0$, the Landau levels are doubly degenerate due to the valley degeneracy of the two Dirac points. When r increases, the two valleys become coupled and the degeneracy is progressively lifted. The spectrum in the vicinity of $\varphi = 1/2$ can be described using semiclassical arguments. It can be obtained from Bohr-Sommerfeld quantization $\mathcal{S} = 2\pi(n+\gamma)eB$, where $\mathcal{S}$ is the area of a cyclotron orbit of energy ϵ in reciprocal space.

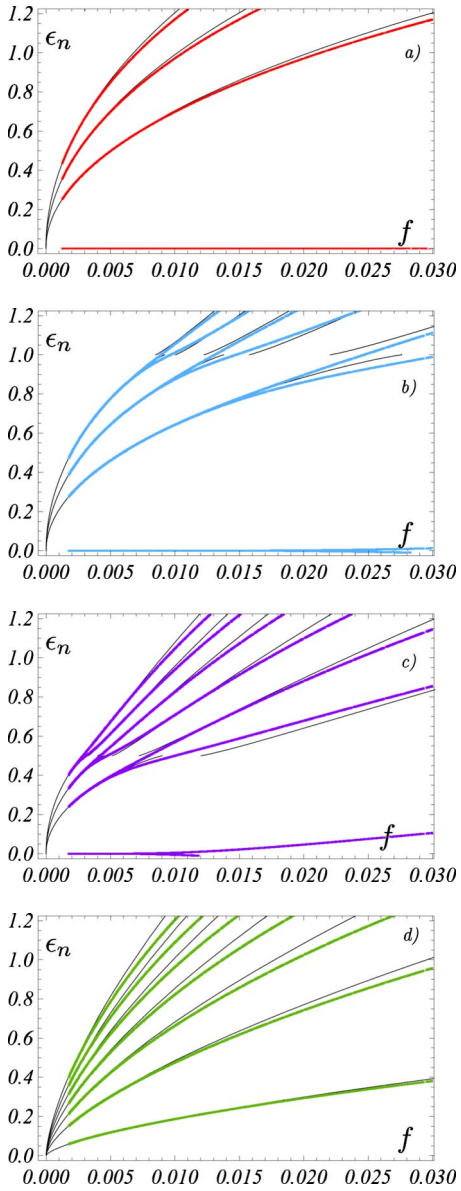

FIG. 7. (Color online) Flux dependence of the energy levels of the tight-binding model on the square lattice, near $\varphi = 1/2$, and for an alternate staggered potential characterized by $r = \Delta_s/2$. (a) The Hofstadter spectrum ($r=0$). (b) $r=.5$ and (c) $r=.75$: the twofold degeneracy of the levels is progressively removed. (d) $r=1$, at the merging of the Dirac cones, the Landau levels vary as $[(n+1/2)f]^{2/3}$. The continuous black lines are the results of the semiclassical quantization, which is quite good except, in the vicinity of the energy $\epsilon = -\Delta = 2(1-r)$. At the merging $r=1$, the energy levels are very well fitted by semiclassical calculation except the ground state for which a numerical factor has been introduced (see text).

We have to distinguish two regimes [Fig. 6(b)]. In the low-energy regime $\epsilon < -\Delta = 2(1-r)$, this is the area enclosed by *one* of the two degenerate isoenergy lines encircling one Dirac point. For the Hamiltonian (1), this area has been calculated in Ref. 9. Moreover, it has been argued that due to a Berry phase $\pm\pi$ around each Dirac point, the mismatch factor γ is 0. Therefore we find

$$\sqrt{\epsilon-\Delta}\left\{(\epsilon+\Delta)K\left[R\left(\frac{\epsilon}{\Delta}\right)\right]-\Delta E\left[R\left(\frac{\epsilon}{\Delta}\right)\right]\right\}=6\pi^2\sqrt{\frac{1+r}{2}}nf, \tag{27}$$

where $K(x)$ and $E(x)$ are complete elliptic integrals of the first and second kinds, respectively,[28] and $R(x)=\sqrt{2x/(x-1)}$. In the limit $\epsilon \ll -\Delta$, one recovers Eq. (26).

In the high-energy regime $\epsilon > -\Delta$ that is above the saddle point, the area enclosed by an isoenergy line encircles *the two* Dirac points so that, due to the cancellation of Berry phases, the mismatch factor γ is now 1/2. The calculation of the area $\mathcal{S}(\epsilon)$ is this regime gives the semiclassical quantization rule

$$\sqrt{\epsilon}\left\{(\epsilon+\Delta)K\left[\frac{1}{R(\epsilon/\Delta)}\right]-2\Delta E\left[\frac{1}{R(\epsilon/\Delta)}\right]\right\}$$
$$=3\pi^2\sqrt{1+r}\left(n'+\frac{1}{2}\right)f. \tag{28}$$

In the limit $\Delta \to 0$, one recovers Eq. (31). It is shown on Fig. 7 that this semiclassical approximation fits very well the numerical calculations, except in the vicinity of the line $\epsilon = -\Delta$ corresponding to the saddle point separating the two Dirac points (Fig. 6).

To go beyond this semiclassical picture, we may explicitly diagonalize the Hamiltonian (25) in a magnetic field. Using the Landau gauge $A_\parallel = Bx$, and performing the Peierls substitution $q_\parallel \to q_\parallel - eBx$, one finds that the eigenvalues ϵ_n are solutions of an effective Schrödinger equation (see details in Refs. 7 and 9)

$$\epsilon_n^2\psi=\left(\frac{m^*\omega_c^2c_\perp^2}{2}\right)^{2/3}[P^2+(\delta+X^2)^2-2X]\psi, \tag{29}$$

where $P=(\frac{2c_\perp}{m^*\omega_c^2})^{1/3}q_\perp$ and $X=(\frac{m^*\omega_c^2}{2c_\perp})^{1/3}x$ are respectively dimensionless momentum and position $[(X,P)=i]$. We have introduced the dimensionless parameter $\delta=\Delta/(\frac{m^*\omega_c^2c_\perp^2}{2})^{1/3}$. In our case, this is a unique function of the flux f and of the parameter r describing the merging

$$\delta=\frac{(r-1)}{\pi^{2/3}(1+r)^{1/3}f^{2/3}}. \tag{30}$$

Equation (29) is an effective Schrödinger equation for a particle in a double-well potential $V(X)=(\delta+X^2)^2-2X$. It has been extensively studied in Ref. 9, where its eigenvalues are plotted as a function of the unique parameter δ. Let us recall here its main characteristics. When $\delta \ll 0$, the two wells of the potential are well separated, one recovers a $\sqrt{nf}$ spectrum of degenerate levels, properly described by Eq. (26), with an excellent fit of the butterfly spectrum near $\varphi=1/2$, $\epsilon=0$ [Fig. 7(a)]. When $-\delta$ is decreased, that is when r or f is increased, the potential barrier between the two wells is reduced, and the tunneling between valleys becomes important. Therefore the twofold degeneracy of the levels is removed, as seen on Figs. 7(b) and 7(c).

When $\delta=0$, that is $r=1$, the spectrum exhibits a single semi-Dirac point. The effective potential $V(X)$ is now a quartic potential $V(X)=X^4-2X$. In Ref. 3, a simple Wentzel-Kramers-Brillouin quantization argument leads to $\epsilon = \pm A(mc_\perp)^{1/3}[(n+1/2)\omega_c]^{2/3}$, where $\omega_c=eB/m^*$ and $A=3^{2/3}\pi/\Gamma(1/4)^{4/3}$. Using the values of the parameters mentioned above, we expect, at the critical point

$$\epsilon = \pm G\left(n'+\frac{1}{2}\right)f^{2/3} \tag{31}$$

with $G=2[36\pi^5/\Gamma(1/4)^4]^{1/3}\simeq 7.99$. This approximation is quite good as soon as $n>1$. However, it has been shown in Ref. 3, that for the ground state, the prefactor has to be multiplied by a factor $g_0\simeq 0.808$.[3] Figure 7(a) shows a remarkable agreement with the semiclassical calculation.

V. CONCLUSION

It is of great interest to study the physics of Dirac points, their motion, and possibly their merging in condensed matter models. In the case of the honeycomb lattice, the motion and merging has been known to be driven by a modification of *hopping parameters* while it is known that a modulated onsite potential opens a gap in the spectrum (like in the case of Boron Nitride) due to parity breaking. Here, we have shown a situation, the Hofstadter problem on a *square lattice* with half-flux quantum per plaquette $\phi_0/2$, where the motion and merging of the Dirac points is not due to a change in the hopping integrals but results from the application of an onsite uniaxial staggered potential. The merging of the Dirac points is discussed within a general Hamiltonian, and the structure of the Landau levels near $\phi_0/2$, is explained quantitatively.

Experimental observation of such a merging could be possible on an optical square lattice of neutral cold atoms, where it has been proposed that massless Dirac Fermions could be obtained in the case of half a flux quantum per plaquette. This can be done by creating gauge fields acting on the internal states of the atoms.[19–21] By adjusting laser parameters appropriately, it is possible to induce a finite phase for the particles moving along a closed path of the lattice. Slightly different scenarios have been proposed in order to reach a state with a Dirac spectrum. In these different scenarios, the merging can then be easily reached by the application of an additional optical potential with the appropriate period $2a$ along one of the main lattice axes. To identify massless Dirac-fermionic spectrum, two methods have already been proposed, Bragg spectroscopy and density-profile measurement. Bragg spectroscopy directly gives access to the dynamic structure factor $S(q,\omega)$. Its dependence on both sides of the merging transition has already been discussed in Ref. 15 for the merging of Dirac points in the honeycomb lattice. The discussion is quite similar for the physical situation discussed here. The density-profile measurement is a time-of-flight experiment. By studying the ballistic expansion of the atomic gas, it is possible to directly access the density of particles. By measuring this quantity as a function of the chemical potential, one obtains the energy dependence of the density of states and its evolution near the merging transition.[15] It has been recently calculated in the framework of the Hamiltonian (1) and can be easily used as a test of the merging.[9]

We became recently aware of a work[29] who proposed that a similar merging could be observed in *d*-wave superconductors. In these systems, the low-energy spectrum exhibits massless Dirac Fermions. In this case, it is found that the merging could be driven in the presence of a charge-density wave (CDW) ordering. It turns out that the description of this merging is quite similar to the problem we are studied here—the Dirac spectrum being due to the *d*-wave superconducting ordering and the alternate potential being provided by a commensurate CDW and could be described within our "universal Hamiltonian."

ACKNOWLEDGMENTS

We acknowledge useful discussions with J. Dalibard, M.-O. Goerbig, and F. Piéchon.

[1] P. R. Wallace, Phys. Rev. **71**, 622 (1947).
[2] For a review see A. H. Castro Neto, F. Guinea, N. M. R. Peres, K. S. Novoselov, and A. K. Geim, Rev. Mod. Phys. **81**, 109 (2009).
[3] P. Dietl, F. Piéchon, and G. Montambaux, Phys. Rev. Lett. **100**, 236405 (2008).
[4] Y. Hasegawa, R. Konno, H. Nakano, and M. Kohmoto, Phys. Rev. B **74**, 033413 (2006).
[5] V. M. Pereira, A. H. Castro Neto, and N. M. R. Peres, Phys. Rev. B **80**, 045401 (2009).
[6] B. Wunsch, F. Guinea, and F. Sols, New J. Phys. **10**, 103027 (2008).
[7] G. Montambaux, F. Piéchon, J.-N. Fuchs, and M. O. Goerbig, Phys. Rev. B **80**, 153412 (2009).
[8] K. Esaki, M. Sato, M. Kohmoto, and B. I. Halperin, Phys. Rev. B **80**, 125405 (2009).
[9] G. Montambaux, F. Piéchon, J.-N. Fuchs, and M. O. Goerbig, Eur. Phys. J. B **72**, 509 (2009).
[10] O. Bahat-Treidel, O. Peleg, M. Grobman, N. Shapira, M. Segev, and T. Pereg-Barnea, Phys. Rev. Lett. **104**, 063901 (2010).
[11] S. Katayama, A. Kobayashi, and Y. Suzumura, J. Phys. Soc. Jpn. **75**, 054705 (2006).
[12] A. Kobayashi, S. Katayama, Y. Suzumura, and H. Fukuyama, J. Phys. Soc. Jpn. **76**, 034711 (2007).
[13] M. O. Goerbig, J. N. Fuchs, G. Montambaux, and F. Piéchon, Phys. Rev. B **78**, 045415 (2008).
[14] S. Banerjee, R. R. P. Singh, V. Pardo, and W. E. Pickett, Phys. Rev. Lett. **103**, 016402 (2009).
[15] S.-L. Zhu, B. Wang, and L.-M. Duan, Phys. Rev. Lett. **98**, 260402 (2007).
[16] E. Zhao and A. Paramekanti, Phys. Rev. Lett. **97**, 230404 (2006).
[17] K. L. Lee, B. Grémaud, R. Han, B.-G. Englert, and C. Miniatura, Phys. Rev. A **80**, 043411 (2009).
[18] N. R. Cooper, Adv. Phys. **57**, 539 (2008).
[19] D. Jaksch and P. Zoller, New J. Phys. **5**, 56 (2003).
[20] F. Gerbier and J. Dalibard, New J. Phys. **12**, 033007 (2010).
[21] J.-M. Hou, W.-X. Yang, and X.-J. Liu, Phys. Rev. A **79**, 043621 (2009).
[22] Non-Abelian gauge potentials have also been suggested, see: K. Osterloh, M. Baig, L. Santos, P. Zoller, and M. Lewenstein, Phys. Rev. Lett. **95**, 010403 (2005); N. Goldman, A. Kubasiak, A. Bermudez, P. Gaspard, M. Lewenstein, and M. A. Martin-Delgado, *ibid.* **103**, 035301 (2009).
[23] D. Hofstadter, Phys. Rev. B **14**, 2239 (1976).
[24] This spectrum had already been obtained in another context: G. Montambaux, International Conference on Synthetic Metals-ICSM 90, Tübingen, Germany, 1990 (unpublished).
[25] D. J. Thouless, Phys. Rev. B **28**, 4272 (1983).
[26] G. E. Volovik, Lect. Notes Phys. **718**, 31 (2007).
[27] J. W. McClure, Phys. Rev. **104**, 666 (1956).
[28] I. S. Gradshteyn, I. M. Ryzhik, and A. Jeffrey, *Tables of Integrals, Series, and Products* (Academic Press, New York, 2007).
[29] A. C. Durst and S. Sachdev, Phys. Rev. B **80**, 054518 (2009).